

**SYNTHESIS AND CHARACTERIZATION OF  
rGO AND TiO<sub>2</sub>/rGO COMPOSITE VIA SPRAY  
PYROLYSIS TECHNIQUE FOR  
PHOTODETECTOR APPLICATION**

**ALSHAMMARI, ANOUD SAUD A**

**UNIVERSITI SAINS MALAYSIA**

**2021**

**SYNTHESIS AND CHARACTERIZATION OF  
rGO AND TiO<sub>2</sub>/rGO COMPOSITE VIA SPRAY  
PYROLYSIS TECHNIQUE FOR  
PHOTODETECTOR APPLICATION**

by

**ALSHAMMARI, ANOUD SAUD A**

**Thesis submitted in fulfillment of the requirements  
for the degree of  
Doctor of Philosophy**

**October 2021**

## ACKNOWLEDGEMENT

I endured easy and difficult, good and thought-provoking times in the course of this research, hence I would like to thank Allah Almighty for His mercy, bounty and for granting me health, patience and the will power to satisfactorily carry out this research. I would like to express my sincere gratitude and appreciation to my main supervisor, Dr Mohd Mahadi Halim, and co-supervisors, Assoc. Prof. Dr Yam Fong Kwong and Dr Noor Haida Mohd Kaus for their expert guidance's, valuable assistance, motivation and immense knowledge towards the realization of this study. Their enormous knowledge has helped me a lot throughout my research work. I would also like to acknowledge generally, Universiti Sains Malaysia (USM) for the availability of the needed facilities and specifically, partial support from RUI grant under School of Physics, USM (1001/PFIZIK/8011092) which enable the success of my project. I am also very much grateful to the University of Northern Border University, Rafha, Saudi Arabia, which provided me scholarship and allowed me to further study in USM. Very special thanks go to all staff of the School of Physics, USM, which has contributed enormously throughout my study. I also want to thank all my friends and colleagues who supported me and helped me at the School of Physics, USM. Last but not least, my deepest appreciation dedicated to my parents, sisters and brothers for their love, support, patience and faith in me. All my accomplishments will not be possible without them in my life.

Anoud Alshammari  
2021  
Penang, Malaysia

## TABLE OF CONTENTS

<b>ACKNOWLEDGEMENT</b> .....	<b>ii</b>
<b>TABLE OF CONTENTS</b> .....	<b>iii</b>
<b>LIST OF TABLES</b> .....	<b>vii</b>
<b>LIST OF FIGURES</b> .....	<b>viii</b>
<b>LIST OF ABBREVIATIONS</b> .....	<b>xii</b>
<b>LIST OF SYMBOLS</b> .....	<b>xiii</b>
<b>ABSTRAK</b> .....	<b>xv</b>
<b>ABSTRACT</b> .....	<b>xvii</b>
<b>CHAPTER 1 INTRODUCTION</b> .....	<b>1</b>
1.1 Research Background .....	1
1.2 Problem Statement .....	4
1.3 Research Questions .....	5
1.4 Objectives of study .....	6
1.5 Originality of the Study .....	6
1.6 Scope of Study .....	7
1.7 Outline of Thesis .....	7
<b>CHAPTER 2 LITERATURE REVIEW AND THEORETICAL BACKGROUND</b> .....	<b>9</b>
2.1 Introduction .....	9
2.2 Introduction of Graphene .....	9
2.2.1 Overview of Graphene .....	10
2.2.2 Properties of Graphene .....	13
2.3 Graphite oxide.....	14
2.3.1 Synthesis of GO and rGO.....	16
2.3.2 Properties of GO and rGO .....	18
2.3.2(a) Mechanical properties .....	22

2.3.2(b)	Electrical properties .....	22
2.3.2(c)	Thermal properties .....	23
2.3.3	Application of GO and rGO .....	24
2.3.4	Selected Techniques for rGO Production and Exfoliation Processes.....	25
2.4	Mechanism of GO for the thermal reduction in different atmospheres .....	29
2.5	Crystal structure and properties of TiO <sub>2</sub> .....	31
2.6	TiO <sub>2</sub> -rGO nanocomposite synthesis.....	32
2.6.1	Simple mixing method .....	33
2.6.2	Sol-gel method.....	33
2.6.3	Other method .....	33
2.7	Thin-Film Deposition.....	34
2.8	Background of spray pyrolysis technique.....	34
2.9	Concept of photodetection .....	35
2.10	Metal-Semiconductor Contact .....	38
2.11	Photodetector parameters .....	40
2.11.1	Photo-Current, Dark-Current and Light-Current.....	40
2.11.2	Responsivity .....	41
2.11.3	Sensitivity .....	41
2.11.4	Response and recovery time.....	41
2.11.5	Current gain .....	42
2.12	MSM UV photodetector based on G, GO and rGO composite with TiO <sub>2</sub> .....	42
<b>CHAPTER 3 METHODOLOGY AND INSTRUMENTATION.....</b>		<b>45</b>
3.1	Introduction.....	45
3.2	Preparation of substrate.....	45
3.3	Deposition Technique .....	48
3.4	Characterization Techniques.....	49

3.4.1	X-ray diffraction analysis .....	50
3.4.2	Field Emission Scanning Electron Microscopy .....	53
3.4.3	Energy Dispersive X-ray analysis .....	55
3.4.4	UV-Visible Spectroscopy .....	55
3.4.5	Raman Spectroscopy .....	57
3.4.6	Radio Frequency Sputtering System .....	59
3.5	Device fabrication and characterization.....	60
<b>CHAPTER 4 RESULTS AND DISCUSSIONS: THE EFFECT OF SUBSTRATE TEMPERATURE.....</b>		<b>63</b>
4.1	Introduction.....	63
4.2	Synthesis of rGO thin film under different substrate temperatures .....	63
4.3	Result and discussion.....	64
4.3.1	XRD Analysis.....	64
4.3.2	FESEM and EDX Analysis .....	67
4.3.3	UV-VIS Spectroscopy .....	71
4.3.4	Raman Spectroscopy Analysis .....	74
4.3.5	Electrical measurements.....	77
<b>CHAPTER 5 RESULTS AND DISCUSSIONS: THE EFFECT OF NUMBER OF SPRAY CYCLE.....</b>		<b>78</b>
5.1	Introduction.....	78
5.2	Synthesis of rGO thin films with different numbers of spray cycles.....	78
5.3	Result and discussion.....	79
5.3.1	XRD Analysis.....	79
5.3.2	FESEM and EDX analysis .....	80
5.3.3	Raman Spectroscopy .....	86
5.3.4	UV-VIS Spectroscopy .....	87
5.3.5	I-V characteristics.....	90

<b>CHAPTER 6</b>	<b>RESULTS AND DISCUSSIONS: EFFECT OF PRECURSOR CONCENTRATION.....</b>	<b>98</b>
6.1	Introduction.....	98
6.2	Synthesis of TiO <sub>2</sub> /rGO thin film at different concentration.....	98
6.3	Result and discussion.....	100
6.3.1	XRD Analysis.....	100
6.3.2	FESEM and EDX analysis .....	102
6.3.3	Raman Spectroscopy .....	104
6.3.4	UV-VIS Spectroscopy .....	106
6.3.5	<i>I-V</i> characteristics .....	109
<b>CHAPTER 7</b>	<b>CONCLUSION AND FUTURE WORK .....</b>	<b>117</b>
7.1	Conclusion .....	117
7.2	Future work.....	119
	<b>REFERENCES.....</b>	<b>120</b>
	<b>LIST OF PUBLICATIONS</b>	

## LIST OF TABLES

	<b>Page</b>
Table 2.1	Advantages and disadvantages for techniques currently used to produce graphene [3]..... 14
Table 2.2	Selected approaches for exfoliation processes ..... 27
Table 2.3	The electrical nature of ideal metal-semiconductor contact [198]..... 39
Table 2.4	Summary table of comparison of the literature review for thin film photodetection parameters based on UV-PDs ..... 44
Table 4.1	Relation between treatment temperature, peak angle and the interlayer distance of the synthesized material ..... 66
Table 4.2	Atomic percentages of carbon and oxygen present in the GO and rGO thin films..... 70
Table 4.3	Parameters of Raman spectra for GO to rGO reduction treated at different substrate temperatures..... 76
Table 5.1	Raman spectra analysis showing the intensity ratio of the D band and G band ( $I_D/I_G$ )for the GO and rGO thin films at different numbers of spray cycles..... 87
Table 5.2	Photoelectric performance of the Al/rGO/Al MSM PD at different applied bias voltages..... 96
Table 5.3	Photoelectric performances of the Al/rGO/Al MSM PD fabricated in this study and photodetectors of other studies..... 97
Table 6.1	The band gap energy values of the synthesized samples as calculated from the Tauc plot..... 108
Table 6.2	The responsiveness, sensitivity values, rise and fall times of the Al/TiO <sub>2</sub> /Al, Al/TiO <sub>2</sub> /rGO/Al (1, 5, 7, and 10wt.%) MSM films-based UVPDs fabricated in this study as well as those reported in literature for other PDs..... 115



## LIST OF FIGURES

		Page
Figure 2.1	Graphene the building block of all graphitic forms, it can be wrapped into a 0D (buckyballs), 1D (nanotubes) and stacked to form the 3D (graphite) structure[2]. .....	12
Figure 2.2	A model of graphene structure [72]. .....	12
Figure 2.3	General chemical modification routes for exfoliated graphene sheets. (a) 1,3-dipolar cycloaddition of in situ-generated azomethine ylides, (b) Bingel cycloaddition, (c) aryl diazonium addition, and(d) azide addition. Reprinted with permission from [86]. .....	16
Figure 2.4	Schematic representation of: (a) Lattice structure and corresponding energy band diagrams of graphene, GO and rGO; and electronic transitions in (b) GO and (c) rGO[119]. .....	21
Figure 2.5	Schematic illustration of the temperature evolution of GO in nitrogen and ambient air [103] .(*Colored: Potential adsorption sites; Black: non-adsorptive species).....	29
Figure 2.6	Crystal structures of TiO <sub>2</sub> ,(a) anatase, (b) rutile and (c) brookite [162]. .....	31
Figure 2.7	Schematic diagram of charge carriers photoexcitation, E <sub>C</sub> is conduction band energy, E <sub>V</sub> is valence band energy, CB is conduction band, VB is valence band, E <sub>G</sub> is bandgap, and $h\nu$ is photon energy [192]. .....	37
Figure 2.8	Diagram illustrates the mechanism of a photodetection process [193]. .....	37
Figure 2.9	Formation of Schottky barrier between metal and p-type semiconductor: a) neutral and electrically isolated, (b) in an ideal contact [199]. .....	40
Figure 2.10	Calculation on response time and recovery time from a pulse photocurrent [203]. .....	42
Figure 3.1	Flowchart of the steps taken for the synthesis and characterization of rGO and TiO <sub>2</sub> /rGO thin films, and the fabrication of MSM photodetector. ....	47
Figure 3.2	Setup for spray pyrolysis system.....	49

Figure 3.3	(a) X-ray Diffractometer (Bruker D8 Advance), (b) Schematic diagram of X-ray tube, and (c) principle of X-ray diffraction [216].	52
Figure 3.4	(a) FESEM (Model: Nova NanoSEM 450), and (b) schematic diagram of FESEM [218].	54
Figure 3.5	Carry series UV-Vis-NIR spectrophotometer [222].	57
Figure 3.6	(a) Raman spectroscopy system, and (b) Principle of Raman spectroscopy [224].	58
Figure 3.7	Top-view images for prepare thin film samples on sputter plate.	59
Figure 3.8	(a) RF sputtering system (Auto HHV500), and (b) schematic diagram of an RF sputtering system [225].	60
Figure 3.9	Top view FESEM image of PD contact showing the finger mask dimension used for MSM PD application.	61
Figure 3.10	Schematic diagram of the <i>I-V</i> measurements of the fabricated (a) Al/rGO/Al MSM photodetector based on rGO thin-film, and (b) Al/TiO <sub>2</sub> -rGO/Al MSM photodetector based on TiO <sub>2</sub> /rGO thin-film.	62
Figure 4.1	Photographic images of the fabricated GO/rGO thin films at different substrate temperatures.	64
Figure 4.2	X-ray diffraction patterns reveal the GO and rGO peaks of thin films deposited at different substrate treatment temperatures: (a) 50, (b) 100, (c) 150, (d) 200, (e) 250, and (f) 300 °C.	66
Figure 4.3	FESEM images of thin films GO to rGO deposited at different substrate treatment temperatures, (a) 50 °C, (b) 100 °C, (c) 150 °C, (d) 200 °C, (e) 250 °C, and (f) 300 °C.	68
Figure 4.4	FESEM images of GO and rGO thin film's cross section deposited at different substrate treatment temperatures.	69
Figure 4.5	EDX analysis of thin films GO to rGO deposited at different substrate treatment temperatures, (a) 50 °C, (b) 100 °C, (c) 150 °C, (d) 200 °C, (e) 250 °C, and (f) 300 °C.	70
Figure 4.6	Absorption spectra of the synthesized samples with various treatment temperatures ( $T_s = 50, 100, 150, 200, 250$ and $300$ °C).	72
Figure 4.7	The $ah\nu$ versus $E_g$ curve of thin films deposited at different substrate temperatures ( $T_s = 50, 100, 150, 200, 250$ and $300$ °C).	72

Figure 4.8	UV-Vis transmittance spectra of thin films deposited at different substrate temperatures ( $T_s = 50, 100, 150, 200, 250$ and $300\text{ }^\circ\text{C}$ ).....	73
Figure 4.9	Raman spectra for GO to rGO reduction treated at different substrate treatment temperatures. ....	76
Figure 4.10	Sheet resistance of GO/rGO thin films deposited at different substrate treatment temperatures. ....	77
Figure 5.1	Images of the fabricated rGO thin films at different numbers of spray varies from 2, 4, 6, 8 and 10 cycles. ....	79
Figure 5.2	XRD pattern of (a) GO, and (b) rGO films prepared at 2, 4, 6, 8 and 10 spray cycles.....	80
Figure 5.3	Top FESEM view of (a) GO, and rGO thin films prepared at (b) 2, (c) 4, (d) 6, (e) 8, and (f) 10 spray cycles.....	82
Figure 5.4	Cross-sectional FESEM view of the rGO thin films prepared at increasing number of (a) 2, (b) 4, (c) 6, (d) 8, and (e) 10 spray cycle.....	84
Figure 5.5	Elemental analysis from EDX spectra of (a) GO, and rGO thin films prepared at (b) 2, (c) 4, (d) 6, (e) 8, and (f) 10 spray cycles.....	85
Figure 5.6	Raman spectra of (a) GO, and (b) rGO thin films prepared with increasing numbers of spray cycle. ....	86
Figure 5.7	UV-Vis absorbance spectra of (a) GO, (b) rGO thin films, transmittance spectra of (c) GO, (d) rGO thin films, and (e) Tauc plot from the UV-Vis analysis of all films.....	89
Figure 5.8	Schematic diagram for the production process of electron-hole pairs for Al/rGO/Al PD, (a) without light, and (b) with UV light. ....	91
Figure 5.9	The $I$ - $V$ plot for Al/rGO MSM PD under UV illumination and without illumination (a) linear scale, and (b) logarithmic scale. ....	92
Figure 5.10	Responsivity values at different applied bias voltages (1, 2, 3, and 4V). ....	93
Figure 5.11	Bias voltage dependent relaxation response curve of Al/rGO/Al MSM PD showing photocurrent response characteristics at varying bias voltages (1 to 4 V).....	95
Figure 5.12	Normalized current-time curves showing the rise and fall times of the Al/rGO/Al MSM photodetector of at varying bias voltages (1 to 4V).....	96

Figure 6.1	Photographs of the fabricated TiO <sub>2</sub> , and TiO <sub>2</sub> /rGO thin films at different concentration (0, 1, 5, 7 and 10) wt.% .....	99
Figure 6.2	The XRD patterns of TiO <sub>2</sub> , TiO <sub>2</sub> /rGO (1 wt.%), TiO <sub>2</sub> /rGO (5 wt.%), TiO <sub>2</sub> /rGO (7 wt.%), and TiO <sub>2</sub> /rGO (10 wt.%). .....	101
Figure 6.3	The FESEM images of (a) TiO <sub>2</sub> , (b) TiO <sub>2</sub> /rGO (1 wt.%), (c) TiO <sub>2</sub> /rGO (5 wt.%), (d) TiO <sub>2</sub> /rGO (7 wt.%), and (e) TiO <sub>2</sub> /rGO (10wt.%). .....	102
Figure 6.4	EDX spectra of (a) TiO <sub>2</sub> , (b) TiO <sub>2</sub> /rGO (1 wt.%), (c) TiO <sub>2</sub> /rGO (5 wt.%), (d) TiO <sub>2</sub> /rGO (7 wt.%), and (e) TiO <sub>2</sub> /rGO (10 wt.%). .....	103
Figure 6.5	Raman spectra of(a) TiO <sub>2</sub> , (b)TiO <sub>2</sub> /rGO (1 wt.%), (c) TiO <sub>2</sub> /rGO (5 wt.%), (d) TiO <sub>2</sub> /rGO (7 wt.%), and (e) TiO <sub>2</sub> /rGO (10wt.%). .....	105
Figure 6.6	The UV-Vis (a) absorption spectra, and (b) transmission spectra of TiO <sub>2</sub> , TiO <sub>2</sub> /rGO (1 wt.%), TiO <sub>2</sub> /rGO (5 wt.%), TiO <sub>2</sub> /rGO (7 wt.%), and TiO <sub>2</sub> /rGO (10 wt.%). .....	107
Figure 6.7	The $ah\nu$ versus $E_g$ curve for pure TiO <sub>2</sub> , TiO <sub>2</sub> /rGO (1 wt.%), TiO <sub>2</sub> /rGO (5 wt.%), TiO <sub>2</sub> /rGO (7 wt.%), and TiO <sub>2</sub> /rGO (10 wt.%). .....	108
Figure 6.8	The $I$ - $V$ plot for MSM photodetector from (a) TiO <sub>2</sub> , (b) TiO <sub>2</sub> /rGO (1 wt.%), (c) TiO <sub>2</sub> /rGO (5 wt.%), (d) TiO <sub>2</sub> /rGO (7 wt.%), and (e) TiO <sub>2</sub> /rGO (10 wt.%). .....	109
Figure 6.9	Bias voltage dependent relaxation response curve of Al/TiO <sub>2</sub> ,Al/TiO <sub>2</sub> /rGO MSM PD showing photocurrent response characteristics at varying rGO concentrations of 1, 5, 7, and 10 wt.% .....	113
Figure 6.10	Normalized $I$ - $t$ curves showing the rise and fall times of the Al/TiO <sub>2</sub> , Al/TiO <sub>2</sub> /rGO MSM PDs at varying rGO concentrations of 1, 5, 7, and 10 wt.% .....	114

## LIST OF ABBREVIATIONS

1D	One Dimensional
2D	Two Dimensional
3D	Three Dimensional
CNTs	Carbon nanotubes
DC	Direct Current
EDX	Energy Dispersive X-Ray Spectroscopy
FESEM	Field Emission Scanning Electron Microscopy
FWHM	Full Width at Half Maximum
G	Graphene
GO	Graphene Oxide
LEDs	Light emitting diodes
MIR	Mid-Infrared
MSM	Metal-Semiconductor-Metal
PD	Photodetector
PDs	Photodetectors
RGO	Reduced Graphene Oxide
SPT	Spray Pyrolysis Technique
TiO <sub>2</sub>	Titanium Dioxide
UV	Ultraviolet
UVPD	Ultraviolet photodetector
UV-Vis	Ultraviolet-Visible
VLS	Vapor-Liquid-Solid
XRD	X-Ray Diffraction

## LIST OF SYMBOLS

Al	Aluminum
Å	Angstrom ( $1 \times 10^{-10}$ m)
A	Ampere
$k$	Boltzmanconstant
$\theta$	Bragg's angle
$C_B$	Conduction band
$L_a$	Crystalline diameter
$D$	Crystallite size
I	Current
$I-V$	Current-voltage
$I_{dark}$	Dark current
°C	Degree Celsius
$t_{fall}$	Fall time
$q$	Electron charge
e-h	Electron-hole
eV	Electron volt
$E_L$	Energy of light source
$E_g$	Energy bandgap
$E_f$	Fermi level
$L$	Full width at half maximum
$G$	Current Gain
$I_D$	Intensity of D band in Raman
$I_G$	Intensity of G band in Raman
$I_{light}$	Light current
$\Phi_M$	Metal work function

$\mu\text{m}$	Micrometer ( $1 \times 10^{-6}$ m)
M	Molar
nm	Nanometer ( $1 \times 10^{-9}$ m)
$T \%$	Optical transmittance
$n$	Order of reflection
$I_{ph}$	Photo current
$h\nu$	Photon energy
$h$	Plank constant
P	Power
$P_{in}$	Power intensity
$R$	Responsivity
$t_{rise}$	Rise time
$I_s$	Saturation current
$\Phi_S$	Semiconductor work function
S	Sensitivity
$T$	Temperature
t	Time
$E_o$	Vacuum energy
$V_B$	Valence band
$E_v$	Valence energy
V	Voltage
W	Watt
$\lambda$	Wavelength
wt%	Weight percentage

**SINTESIS DAN PENCIRIAN rGO DAN TiO<sub>2</sub>/rGO KOMPOSIT MENERUSI  
TEKNIK SEMBURAN PIROLISIS UNTUK APLIKASI PENGESAN  
CAHAYA**

**ABSTRAK**

Antara semua struktur berasaskan karbon, graphene telah menarik minat terbanyak di sebabkan keunggulannya pada keliangan, kekenyalan, kekonduksian, luas permukaan, dan kestabilan. Terbaru, lebih perhatian telah beralih pada filem nipis graphene oksida (GO) di sebabkan oleh sifat struktur dan elektriknya yang luar biasa, yang membolehkannya di gunakan dalam pembuatan sel solar organik, dan berpotensi di aplikasikan dalam penghasilan dan penyimpanan tenaga. Walaubagaimanapun, pelbagai sebatian kimia penurun (hydrazine, sodium borohidrat, dsb.) yang digunakan dalam proses penurunan bagi mencapai graphene oksida terturun (rGO) adalah toksik. Dalam kajian ini, pertamanya pendekatan yang mudah dan kos efektif bagi mensintesis filem nipis rGO dari larutan koloid GO di cadangkan. Filem nipis rGO ini di sintesis atas substrat kaca dengan kaedah semburan pirolisis (SPT) pada suhu substrat berbeza (50, 100, 150, 200, 250, dan 300 °C). Semua sampel yang di sintesis di cirikan oleh teknik yang berbeza termasuk spektroskopi Raman, mikroskop elektron pengimbas pancaran medan (FESEM), analisa pembelauan sinar-X (XRD), spektroskopi sebaran tenaga sinar-X (EDX), dan spektroskopi UV-Vis. Penurunan dari GO ke rGO di dapati bermula selepas 100 °C, seperti yang di sahkan daripada penurunan unsur oksigen dalam EDX. Sementara, kerintangan bagi filem nipis menurun (iaitu kokonduksian meningkat) dengan peningkatan suhu. Keduanya, kesan kitaran semburan di kaji terhadap sifat morfologi, struktur, dan optik pada bilangan kitar semburan yang berbeza (iaitu dari 2 hingga 10). Analisa optik menunjukkan yang tenaga jurang jalur bagi filem



nipis GO dan rGO berkurang dari 4.2 ke 3.27 eV sebagaimana kitar semburan di tingkatkan dari 2 ke 10, yang mana mengesahkan kesan ketebalan permukaan penglitup keatas kekonduksian. Bagi menguji prestasi filem nipis rGO sebagai peranti pengesan cahaya ultra lembayung (UVPD), konfigurasi logam-semikonduktor-logam (MSM) telah di capai dengan menggabungkan logam Al menggunakan percikan RF keatas sampel filem nipis di sediakan pada 10 kitar semburan. Sebagai tambahan, filem nipis rGO yang di sintesis dengan 10 kitar semburan ini menunjukkan ketebalan 188.54 nm serta bersifat fotoelektrik yang cemerlang (gandaan arus pada 2.318, kepekaan pada 131.84%, sambutan pada 0.0284 A/W, dan masa naik/turun pada 0.055/0.06 s). Ketiganya, kesan kepekatan GO pendahulu pada prestasi pengesanan cahaya bagi MSM UVPD berasaskan TiO<sub>2</sub> dan TiO<sub>2</sub>/rGO di kaji. Filem nipis TiO<sub>2</sub>/rGO dengan kepekatan GO berbeza (1, 5, 7 and 10 wt.%) di mendapkan atas substrat kaca menggunakan SPT. Kejayaan antaramuka di antara TiO<sub>2</sub> dan rGO disahkan dari pelebaran puncak pencirian XRD bagi TiO<sub>2</sub> anatase, peningkatan nisbah keamatan jalur *D* dan *G* ( $I_D/I_G$ ) spektra Raman dari 1.05 ke 1.9, dan penurunan keamatan spektra penghantaran apabila kepekatan rGO meningkat dari 1 ke 10 wt.%. Penurunan pada tenaga jurang jalur filem nipis dari 3.60 ke 3.04 eV dengan peningkatan kepekatan rGO membuktikan kesan kepekatan, dan masa naik dan turun bagi Al/TiO<sub>2</sub>/rGO (10 wt.%) MSM UVPD di tentukan pada 2.11 (A/W), 103.6, 10265 %, 0.057 s, dan 0.055 s, masing-masing, yang mana adalah lebih baik secara relatifnya berbanding yang di laporkan pada kajian terdahulu. Nilai optimum dari peranti yang di fabrikasi ini menandakan bahawa filem nipis TiO<sub>2</sub>/rGO di sediakan dengan kaedah SPT adalah bahan berpotensi bagi pembuatan MSM UVPD berkualiti tinggi dan mengesahkan kesan kepekatan GO ke atas prestasi pengesanan cahaya.

**SYNTHESIS AND CHARACTERIZATION OF rGO AND TiO<sub>2</sub>/rGO  
COMPOSITE VIA SPRAY PYROLYSIS TECHNIQUE FOR  
PHOTODETECTOR APPLICATION**

**ABSTRACT**

Among all new carbon-based structures, graphene has drawn the most attention because of its superiority in terms of porosity, elasticity, conductivity, surface area and stability. Recently, more attention has turned to graphene oxide (GO) thin films due to their exceptional structure and electronic properties, which enables their use in the manufacture of organic solar cells, photonic devices and potential applications in energy production and storage. However, the various reductive chemical compounds (hydrazine, sodium borohydride, etc.) in the reduction process to achieve reduced graphene oxide (rGO) are toxic. In this study, firstly a facile and cost-effective approach to synthesize rGO thin film from GO water dispersion were proposed. The rGO thin films were synthesized on glass substrates by means of spray pyrolysis technique (SPT), under different substrate temperatures (50, 100, 150, 200, 250, and 300 °C). All the synthesizes samples were characterized by different techniques such as Raman spectroscopy, field emission scanning electron microscopy (FESEM), X-ray diffraction analysis (XRD), energy-dispersive X-ray (EDX) spectroscopy, and UV–Vis spectroscopy. The reduction of GO to rGO was found initiated after 100 °C, as confirmed by the decrease in oxygen element shown by the EDX. While the resistance of the thin films decreased (i.e. conductivity increases) with increase in temperature. Secondly, the effect of spray cycles was studied on the morphological, structural, and optical properties under numbers of spray cycles (i.e. 2 to 10). The optical analysis showed that the energy band gap of GO and rGO thin films were

reduced from 4.2 to 3.27 eV as the spray cycles increased from 2 to 10, which confirms the effect of surface coating thickness on conductivity. To test the performance of the rGO thin film as a UV photodetector (UVPD) device, metal-semiconductor-metal (MSM) configuration was achieved by incorporating Al metal using RF sputtering on the thin film sample prepared with 10 spray cycles. Moreover, the rGO thin film synthesized with 10 spray cycles displayed a thickness of 188.54 nm and excellent photoelectric properties (current gain of 2.318, sensitivity of 131.84%, responsivity of 0.0284 A/W and rise/fall times of 0.055 s/0.06 s). Thirdly, the effect of GO precursor concentration on the performance of MSM UVPD based on TiO<sub>2</sub> and TiO<sub>2</sub>/rGO films were studied. TiO<sub>2</sub>/rGO thin films with different concentrations of GO (1, 5, 7 and 10 wt%) were deposited on the glass substrates via SPT. The successful interface between TiO<sub>2</sub> and rGO was confirmed by the broadening of the characteristic XRD peak for anatase TiO<sub>2</sub>, increasing *D* and *G* band intensity ratios (*I<sub>D</sub>/I<sub>G</sub>*) of Raman spectra from 1.05 to 1.9, and decreasing intensity of UV-Vis transmittance spectra as the GO concentration is increased from 1 to 10 wt.%. The decline in the energy bandgap of the TiO<sub>2</sub>/rGO thin films from 3.60 to 3.04 eV with increase in GO from 1 to 10 wt.%, proves the effect of GO concentration on conductivity. The photoresponsivity, current gain, sensitivity, and rise and fall times of Al/TiO<sub>2</sub>/rGO (10 wt.%) MSM UVPD were determined to be 2.11 (A/W), 103.6, 10265 %, 0.057 s, and 0.055 s, respectively, which are relatively better than those reported in previous studies. These optimum values of the fabricated device indicate that TiO<sub>2</sub>/rGO thin film prepared via SPT is a promising material for a high quality MSM UVPD and confirms the effect of GO concentration on the photodetection performances.

# CHAPTER 1

## INTRODUCTION

### 1.1 Research Background

In recent years, new carbon-based structures such as carbon nanotubes, nanowires and graphene, have drawn great attention because of their intrinsic features and potential applications. Among all the structures, graphene has gathered the most attention due to its structure stability, porosity, elasticity, conductivity, and large surface area. The stability of graphene structure is due to  $sp^2$  hybridized carbon-carbon (C-C) bonds [1]. The bonds are stronger, which are present within the plane, while empty orbitals exit out of the plane. In the structure, one carbon is attached to the other three carbons, while the fourth electron is free to move, and it is responsible for electronic conduction. Moreover, as a single two-dimensional atomic layer of  $sp^2$  bonded carbon atoms [2], graphene has been established as a promising material [3] due to its unique and superior electrical [4], mechanical [5], and thermal properties [6].

Meanwhile, graphene oxide (GO) is an atomic sheet of graphite affixed to several oxygenated functional groups on its basal planes and edges, resulting in a hybrid structure containing a mixture of  $sp^2$  and  $sp^3$  hybridized carbon atoms [7]. The formation of  $sp^3$  domains in GO is attributed to the oxidation reaction, which results in hybridized carbon atoms (covalently bonded) attached to different types of functional groups, such as epoxide, hydroxyl, carboxyl and carbonyl [8, 9].

GO can be synthesized by the oxidation of graphite into graphite oxide, followed by the exfoliation of this graphitic oxide into GO [10]. Recently, more attention has turned to GO thin films due to their exceptional structure [11] and electronic properties [12], which enables their use in the manufacture of organic solar

cells. GO is known as an intermediate phase in the chemical synthesis of reduced graphene oxide (rGO), where the oxygen functional groups within the GO structure are removed thermally or chemically. Recently, researchers' attention has also focused on GO and rGO nanocomposites, which lead to the development of various applications [13].

Several techniques are used to synthesize rGO thin films. These includes sol-gel deposition [14], electrophoretic deposition [15], chemical bath deposition [16], and spray pyrolysis technique (SPT) [17, 18]. SPT is a well-known technique for manufacturing nano range moieties with the advantage of homogeneous deposition of thin film material on glass substrate.

The SPT is a versatile technique for producing functional materials on the industrial and laboratory scale [19-22]. SPT is a frequently applied for the synthesis of transparent and conductor oxides due to its facile procedure, non-vacuum system of deposition and large area of deposition [23]. Its advantages also include low cost, relative simplicity, controllable size, reproducible with continuous operation, and short processing time. In SPT, a thin film is deposited by spraying a solution onto a heated surface, where the constituents react to form a chemical compound. The chemical reactants are selected such that the products other than the desired compound are volatile at the temperature of deposition. Among essential graphene and its derivatives, rGO outperforms graphene and GO on account of its rich functional groups and excellent conductivity [24-26].

The rGO thin film exhibits remarkable characteristics in the areas of photodetector, gas sensor, and other applications [27, 28]. The advantages rGO include cheap synthesis, good dispersion in organic solvents, and well attuned to a wide array

of organic and inorganic semiconductors [29]. These unique characteristics of rGO allow for its functionalization with other organic materials for photocatalytic, photodetector, and photovoltaic applications [30-34]. For instance, rGO has been conjugated with  $\text{WO}_3$  for enhanced charge transfer and improved photodetection capabilities [35]. Recent studies demonstrate that rGO is a viable material for efficient load transfer and high photo response for inorganic semiconductor materials because of its extraordinary weak electron affinity ( $\sim 4.5$  eV) [36]. The photo-catalytic activity of  $\text{TiO}_2/\text{rGO}$  is several times higher than pure  $\text{TiO}_2$  [37]. Currently,  $\text{TiO}_2/\text{rGO}$  nanocomposites are being synthesized to improve the performance of solar cells, photocatalysts, photodetectors and lithium-ion batteries [38-41].

Semiconductor photodetectors have demonstrated immense potential for ultraviolet photodetection application on account of their cost effectiveness and facile requirements. In recent times, ultraviolet photodetectors (UVPDs) are globally recognized due to their prospective applications in solar UV radiation detection, in situ combustion gas monitoring, gas sensing, combustion engine control, flame monitoring, missile detection, UV treatment, biological, and chemical sensors [42-45]. Nanostructure materials like SiC,  $\text{V}_2\text{O}_5$ , GaN, AlGaIn,  $\text{Nb}_2\text{O}_5$ ,  $\text{TiO}_2$  and ZnO have been utilized to fabricate UV PDs because of their wide energy bandgap [46-51]. Moreover, metal oxide semiconductors PDs are inexpensive, easy to fabricate and highly sensitive/responsive in the UV region [47-50]. To improve their sensitivity, variations of nanomaterial-based UV detectors have been developed, such as metal-semiconductor-metal (MSM) structure [52], Schottky photo barrier photodiodes [53], and composite with organic materials [54]. On the other hand, heterojunction forming of  $\text{TiO}_2$  with other semiconductors ( $\text{C}_3\text{N}_4$ ,  $\text{WO}_3$ , ZnS etc.) [55, 56], carbon materials - carbon nanotubes, graphene, GO, rGO, fullerene and metal nanoparticles have shown

to be very effective in reducing surface recombination [32, 52, 54, 57-60]. This has prompted the intensity of research on the fabrication of optoelectronic devices based on reduced rGO [61]. Therefore, this study proposes the synthesis of TiO<sub>2</sub>/GO composite using SPT to enhance increase sensitivity of photodetector sensitivity.

## 1.2 Problem Statement

Despite the significant progress in the use of solution-based nanostructured metal-oxide semiconductors for various application including photocatalytic systems, solar cells, and photodetectors, they have some limitations to be used for large-scale application which are:

- (i) wide band gap energy,
- (ii) high charge carrier recombination rate, and
- (iii) small surface area.

Various approaches have been executed to solve these downsides in order to enhance the photoactivity for the nanostructured metal-oxide semiconductors. One of these methods is to load metal-oxide semiconductor on graphene sheets to increase the charge separation, decrease its band gap and increase its surface area. Graphene, known as a novel carbonaceous material of two-dimensional (2D) with atom-thick layer properties and honeycomb crystal structure, has become the best in the carbon group, displays prominent physical, chemical features and excellent electrocatalytic capability. Many preceding investigations have assured that introducing graphene to the nanostructured metal-oxide semiconductor could greatly enhance the photo-efficiency. This enhancement of photo-efficiency is due to three reasons. The first reason is graphene decreases the charge carrier (electron-hole pairs) recombination rate. The second one is graphene narrow the band gap of semiconductor. The third

reason is that graphene significantly enhances the surface area of the nanostructured metal-oxide semiconductor. There is a problem in synthesizing nanostructured metal-oxide semiconductor/graphene nanocomposites in aqueous solutions which is originated by the agglomeration of graphene sheets in aqueous solutions due to Van der Waals interaction. So, rGO has been vigorously used to couple with various nanostructured metal-oxide semiconductor forming highly stable dispersion of photo-active nanostructured metal-oxide/rGO nanocomposite using GO as starting material. Synthesis of the photo-active nanostructured metal-oxide/rGO nanocomposite is mostly conducted by methods of chemical and thermal reduction of GO nanostructured metal-oxide dispersion in an inert gas environment. Nonetheless, usually, these methods require expensive equipment, toxic reduction agents and complicated preparations conditions. Thus, it is highly desirable to introduce scalable synthetic strategy to fabricate highly photo-active nanostructured metal-oxide/rGO films using an aqueous GO dispersion as a starting material.

### **1.3 Research Questions**

- (i) How to fabricate rGO thin films from stable GO colloidal solution via SPT?
- (ii) What is the effect of substrate temperature on the morphological, structural, and optical properties of the rGO thin films synthesized using SPT?
- (iii) What is the effect of number of spray cycles on the morphological, structural, and optical properties of the rGO thin films synthesized using SPT?



- (iv) What is the effect of precursor GO concentration on the photoelectric properties and photodetection performance of TiO<sub>2</sub>/rGO based ultraviolet photodetector UVPD?

#### **1.4 Objectives of study**

The specific objectives of this study are summarized in the following points:

- (i) To fabricate rGO films by spray pyrolysis technique using aqueous GO dispersion as a starting material.
- (ii) To investigate the effect of substrate temperature on the synthesis of rGO thin films without any toxic reducing agent.
- (iii) To characterize the synthesized rGO thin films prepared under different spray cycles (2, 4, 6, 8 and 10).
- (iv) To evaluate the performance of the fabricated MSM UVPDs device based on TiO<sub>2</sub> and TiO<sub>2</sub>/rGO thin films at rGO concentrations (0, 1, 5, 7 and 10 wt.%).

#### **1.5 Originality of the Study**

This is the first study carried out to convert the stable colloidal GO to rGO thin films by using SPT at a lower temperature (150 °C) without any toxic reducing agent. In this work, rGO thin films were deposited on glass substrate at different deposition cycles (2, 4, 6, 8 and 10). The structural, optical and morphological properties of the as-prepared rGO thin films were analyzed using an array of measurements. The study of the effect and optimization of spray cycles on morphological, structural and optical properties of the rGO thin films is a novel

approach, as well as the effect of precursor GO concentration (1, 5, 7, and 10 wt.% ) on the performance of TiO<sub>2</sub>/rGO thin film-based UV PD.

## **1.6 Scope of Study**

In this research work, rGO thin films were fabricated by using SPT at different substrate temperatures ( $T_s = 50, 100, 150, 200, 250, \text{ and } 300 \text{ }^\circ\text{C}$ ). The work involves the deposition of rGO thin films on glass substrates via SPT at different spray cycles (2 to 10). This study proposed a cost-efficient approach of fabricating a high-performance rGO based MSM UV photodetector at optimum spray cycle. This study evaluates the photodetection performance of MSM UVPD based on pure TiO<sub>2</sub> and TiO<sub>2</sub>/rGO films deposited on glass substrates. TiO<sub>2</sub>/rGO thin films with different concentrations of GO (1, 5, 7, and 10 wt.%) were deposited on glass substrates using SPT. The characterization of photoelectric properties will help to validate TiO<sub>2</sub>/rGO thin film prepared via SPT as a promising material for the manufacture of high quality MSM PDs. The effect of GO concentration on the photodetection performance was also investigated.

## **1.7 Outline of Thesis**

Chapter 1 contains overview graphene, GO, rGO, and SPT. The research problem, research questions, the research objectives and research originality are also included in this chapter. Chapter 2 reviews pertinent studies and provides theoretical background of this study and its fundamental principles. Chapter 3 describes the experimental equipment, and characterization instruments used in the preparation of rGO thin films and fabrication of photodetection device. Chapter 4 describes the fabrication process, characterization techniques and results of the prepared rGO thin

films at different temperature. Chapter 5 explains the synthesis of the rGO thin films at different cycles and discusses the fabrication of photodetector at optimum spray cycle (i.e. 10). Chapter 6 focuses on the photodetection properties of pure TiO<sub>2</sub> and TiO<sub>2</sub>/rGO based MSM photodetector, and confirms the effect of GO concentration on the photodetection performance. Chapter 7 summarizes the research findings and presents recommendation for future work and the research contribution.

## CHAPTER 2

### LITERATURE REVIEW AND THEORETICAL BACKGROUND

#### 2.1 Introduction

This chapter provides a synopsis of graphene, GO, and rGO material, which covers their properties, preparation/synthesis, as well as applications. As part of this study, the crystal structure and properties of TiO<sub>2</sub> were also reviewed. Also reviewed is the deposition of GO, rGO, and rGO/TiO<sub>2</sub> thin films using different methods. In addition, the basic principles of metal–semiconductor contacts and MSM PDs were concisely described in this chapter.

#### 2.2 Introduction of Graphene

Carbon has several polymorphs, and these include diamond, graphite, and amorphous carbon. While diamond and graphite are well established allotropes of carbon, fullerene and carbon nanotubes CNTs were discovered by Kroto et al., in 1985, and Iijima in 1991, respectively. Thus, three-dimensional (3D) (diamond and graphite), one-dimensional (1D; CNTs), and zero-dimensional (0D; fullerenes) allotropes were well recognized in the carbon community. However, it was realized in 1991 that CNTs were actually formed by rolling a two-dimensional 2D graphene sheet, which is a single layer from a 3D graphitic crystal. Nonetheless, the isolation of graphene was quite elusive, hence the dearth of experimental research on graphene until 2004.

Graphene is the basic structural component of some carbon allotropes, including graphite, CNTs, and fullerenes. Fullerene wholly comprises spherically shaped carbon referred to as bucky balls, while CNTs have tubular forms.

For over 20 years, fullerene and CNTs-based materials benefitted from extensive applications in different areas of research such as electronics, batteries, supercapacitors, fuel cells, electrochemical sensors, biosensors, and therapeutic applications. Presently, graphene has evolved into a “rising star” material after its successful synthesis in 2004 by Andre Geim and his coworkers using a simple scotch tape approach. Graphene consists of a single-layer sheet of  $sp^2$  bonded carbon atoms with a densely packed honeycomb crystal lattice. Its remarkable features include high surface area, tunable band gap, room temperature Hall effect, and exceptional electrical, thermal, and conductive properties, which provide a versatile platform for its utilization as an active material in the synthesis of a range of composite materials [4]. The structure, preparation, properties, and applications of graphene and its composite materials have been reviewed in several studies [2, 62-64]. In recent times, graphene has developed into one of the most sought-after materials. It can be utilized in diverse applications and for the manufacture of a variety of devices because of the listed exceptional properties.

### **2.2.1 Overview of Graphene**

Graphene is a flat monolayer of carbon atoms densely packed into a 2D honeycomb lattice. It is the fundamental unit for graphitic materials of all other dimensionalities, as depicted in Figure 2.1. Graphene has distinctive physical, chemical and mechanical properties [2, 65]. It is the first identified 2D material that has a singular band structure where the valence and conduction bands touch each other [66].

Graphene is typically found in nature in the form of graphite, which is simply a stack of graphene layers bonded by Van der Waals interactions [67]. Graphene has garnered immense attention from the research community [68, 69] because of its potential application in the manufacture of electrochemical devices, and heat insulators. It is also a transparent and flexible semiconductor, which makes it a viable substitute for the relatively costly indium tin oxide (ITO) [68-70]. Theoretically, graphene is the hardest material owing to its  $sp^2$  carbon-carbon bond arrangement [2]. It has a high electron mobility, implying that electrons can travel unrestricted through it for lengthy distances, which makes it a very alluring material for fast transistors [4]. The structure of graphene is depicted in Figure 2.2. Graphene presumably does not exist as a free standing material because of its thermodynamic instability [68]. It has a one atom thick layer of carbon atoms sheet bonded to each other via  $sp^2$  hybridization [71]. The monolayer structure of graphene has been confirmed using Raman spectroscopy [4]. The structure of graphene is depicted in Figure 2.2. Graphene has unique physical, chemical and mechanical properties [71]. It is the first known two-dimensional material which has a singular band structure, and its valence band and conduction band are touching each other [72]. Graphene was presumably thought does not exist as a free standing material because of its thermodynamic instability [68]. It has a one atom thick layer of carbon atoms sheet bonded to each other via  $sp^2$  hybridization [73].

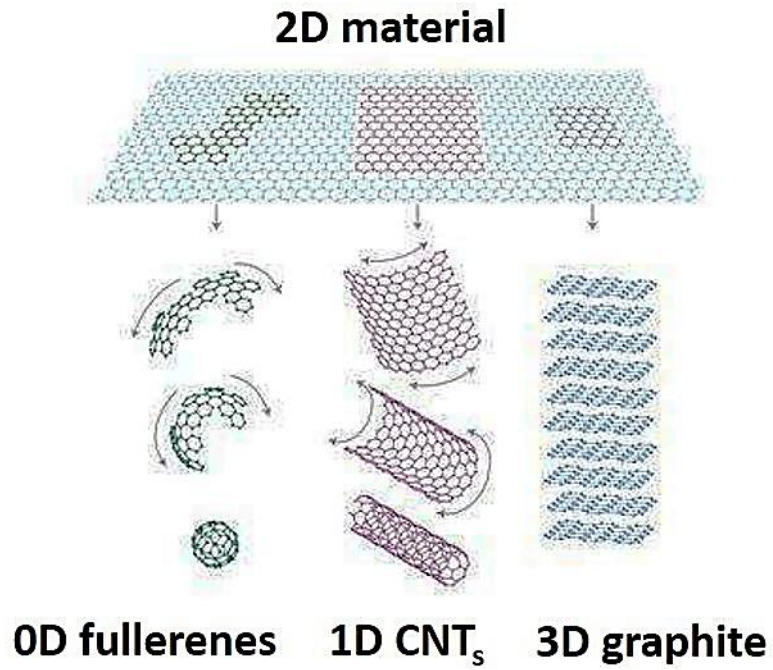


Figure 2.1 Graphene the building block of all graphitic forms, it can be wrapped into a 0D (buckyballs), 1D (nanotubes) and stacked to form the 3D (graphite) structure[2].

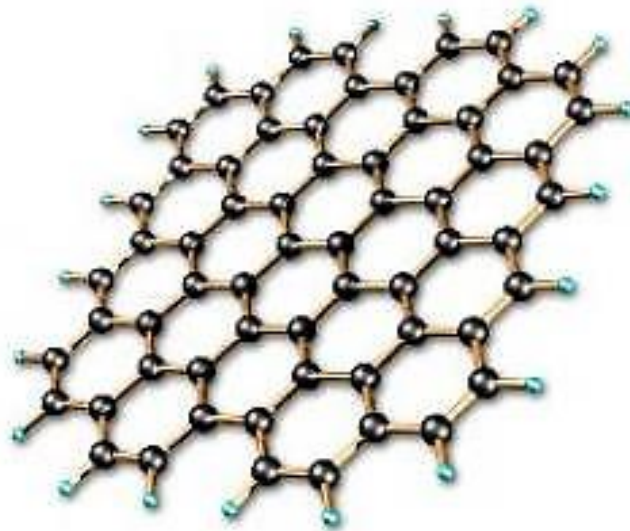


Figure 2.2 A model of graphene structure [72].

### 2.2.2 Properties of Graphene

The C-C bond in graphene has a bond length of approximately 1.42 Å. Graphene is characterized by a strong bond in a specific layer but weak interlayer bonding. Graphene has a specific surface area (of a single sheet) of  $\sim 2630 \text{ m}^2/\text{g}$ , transmittance  $>97.7\%$ , band gap value of  $\sim 0-0.25 \text{ eV}$ , high carrier mobility ( $\sim 200,000 \text{ cm}^2/\text{Vs}$ ), and high Young's modulus (1.0 TPa) [73]. Based on these unique physical and optical properties, graphene and its composite materials can be used as semiconductors.

Graphene has been envisaged as the fundamental unit of all other essential graphitic allotropes such as graphite-stacked version of graphene; CNT-rolled version of graphene, and fullerene-wrapped version of graphene. The exceptional magnetic properties of nanographene e.g. edge-state spin gas probing, magnetic switching, and spin glass states, have been investigated for potential applications in electronic and magnetic devices [74].

Nonetheless, for a quick reference regarding the synthesis of graphene, Table 2.1 presents the benefits and constraints of different synthesis techniques [3].



Table 2.1 Advantages and disadvantages for techniques currently used to produce graphene [3].

	<i>Advantages</i>	<i>Disadvantages</i>
Mechanical exfoliation	(i) Low cost and simplicity (ii) No special equipment needed, (iii) SiO <sub>2</sub> thickness is tunable for better contrast	(i) Uneven films (ii) Labor intensive (not suitable for large-scale production of graphene)
Epitaxial growth	(i) Produces the most homogeneous films (compared to other methods) (ii) Large-scale area	(i) Complex control of morphology and adsorption energy (ii) Requires high temperature
Reduction of graphene oxide	(i) Simple to upscale (ii) Flexible handling of the suspension (iii) Fast process	(i) Fragile stability of the colloidal dispersion (ii) Reduction to graphene is incomplete

### 2.3 Graphite oxide

Graphite oxide is characterized by a layered structure resembling that of graphite. Although the exact structure of GO is difficult to determine, it is clear that for GO the previously contiguous aromatic lattice of grapheme is interrupted by epoxides, alcohols, ketones, and carboxylic groups. The interruption of the lattice is reflected by an increase in interlayer spacing from 0.335 nm for graphite to more than 0.625 nm for GO [75]. Under ultrasonication, these oxidized layers could lead to exfoliation in water. In cases where the exfoliated sheets has only a single or a small number of layers of carbon atoms like graphene, then these sheets are called GO [4]. Therefore, graphite oxide is a single-atomic-layered material composed of carbon, hydrogen, and oxygen molecules. The oxygen component is derived from the oxidation of graphite crystals, as illustrated in Figure 2.3 [76]. Graphite oxide are inexpensive, abundant, easy and economical to synthesize and dispersible in water. Most notably, GO can be partially reduced to graphene-like sheets through the removal

of the oxygen-bearing groups, and with the recovery of a conjugated structure.

The reduced version of GO, sheets are typically regarded as a type of chemically derived graphene and are referred to as rGO. The rGO has also been named functionalized graphene, chemically modified graphene, chemically converted graphene, or reduced graphene [77-80]. GO has two major properties: (i) it can be synthesized using cheap graphite as the precursor material via economical chemical approaches with a high yield and (ii) it is very hydrophilic and can form stable aqueous colloids to enable the assembly of macroscopic structures by means of facile and economical solution processes.

The graphene sheet comprises only trigonally bonded  $sp^2$  carbon atoms and is perfectly flat [81], apart from its microscopic ripples. The heavily decorated GO sheets consist partly of tetrahedrally bonded  $sp^3$  carbon atoms, which are displaced slightly above or below the graphene plane [82]. Due to structural defects and the incidence of covalently bonded functional groups, GO sheets are atomically uneven [83]. A number of studies have examined the surface of GO and discovered highly defective/disordered sections that possibly resulting from the presence of oxygen, and other regions are almost completely intact [84]. It has been reported that the graphene-like honeycomb lattice in GO is preserved, although with a disorder that is, the carbon atoms affixed to/conjugated with functional groups are somewhat displaced, while the general size of the unit cell in GO stays similar to that of graphene [85]. Therefore, GO can be explained as a randomized distribution of oxidized areas with oxygen-containing functional groups combined with nonoxidized regions where most of the carbon atoms are bonded via  $sp^2$  hybridization. The study of GO and rGO is trendy subject in the research and development of graphene, particularly with regards to mass applications of graphene.

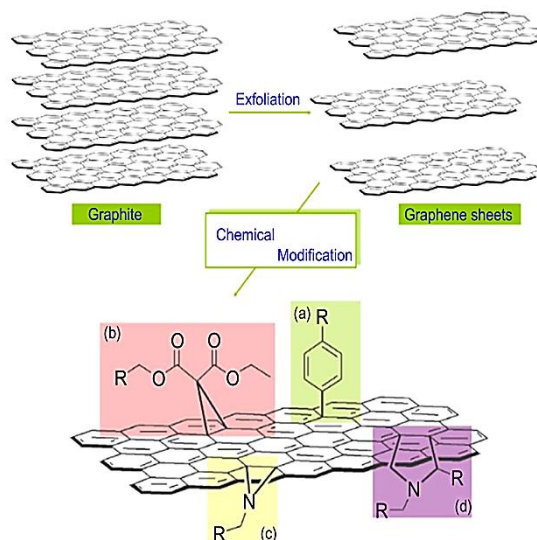


Figure 2.3 General chemical modification routes for exfoliated graphene sheets. (a) 1,3-dipolar cycloaddition of in situ-generated azomethine ylides, (b) Bingel cycloaddition, (c) aryl diazonium addition, and (d) azide addition. Reprinted with permission from [86].

### 2.3.1 Synthesis of GO and rGO

Graphite is a 3D carbon-based material that consists of millions of graphene layers. Through the oxidation of graphite with strong oxidizing agents, oxygenated compounds can be introduced in its structure, which expands the interlayer/interplanar spacing and makes the material hydrophilic (i.e., enable dispersion in water) [85]. The hydrophilic feature enables the graphite oxide to be exfoliated in water via sonication, eventually generating single-layer graphene or graphene with a few layers, referred to as GO. GO can either be reduced to a thin film or in an aqueous solution. Several of the current methods of synthesizing GO are anchored in the method first reported by Hummers wherein graphite is oxidized by a solution of potassium permanganate in sulfuric [87].

Hydrazine is commonly utilized for the reduction of GO, but it is highly toxic

and can potentially functionalize GO with nitrogen heteroatoms [88]. Due to these limitations of hydrazine, more viable options are being used such as  $\text{NaBH}_4$  [89], ascorbic acid [90], and HI [91, 92].

Graphite oxide and GO have similar chemical properties, but with structural difference [93]. The major disparity between graphite oxide and GO is the interplanar spacing between the individual atomic layers of the compounds, which is due to water intrusion [93]. This expanded interlayer spacing due to oxidization, also disrupts the  $\text{sp}^2$  bonding configuration, which explains the reason both graphite oxide and GO are frequently portrayed as electrical insulators [93]. Although graphite oxide is a multilayer system in GO dispersion, a few layers or monolayer of flakes can be found [94]. GO is a poor conductor but its treatment with light, heat, or chemical reduction can restore most features of the well-known pristine graphene.

A few methods are employed to transform graphite oxide into GO. The most widely used methods include sonication, stirring, or a combination of the two. Sonication can be a very time-effective method of exfoliating graphite oxide, and has proven to be extremely efficient at exfoliating graphene; however, it can also seriously damage the graphene flakes and reduce their surface size from microns to nanometers, and it also leads to the production of graphene with disproportionate platelet sizes [95].

The reduction of GO to rGO is a very critical process because it plays a significant role on the quality of the rGO by determining the structural similarity between rGO and pristine graphene [96]. In extensive operations where scientists and engineers are required to use vast amounts of graphene for industrial applications such as energy storage, rGO is the most apparent solution due to the relative simplicity in synthesizing adequate quantities of graphene at the preferred levels of quality [97].

There are several chemical, thermal, or electrochemical approaches to graphene reduction. Although a number of these techniques can produce very high-quality rGO, similar to pristine graphene, they can be complex or protracted [98].

There are several paths to retrieve the graphene-like structure from GO. Among them, two common methods are chemical reagent reduction and thermal reduction. Compared to the latter, reduction via chemical reagents is hindered by toxicity, elemental impurities and environmental impact of some reducing agents, such as sodium borohydride [99], or hydrazine [100]. Hence, thermal treatment to convert GO to rGO has attracted attention as it is a fast, easy, non-toxic, and can be incorporated in manufacturing processes [101, 102]. Thermal treatment of GO into rGO is an intricate mechanism that involves successive phases of water evaporation, removal of groups, and decomposition of carbon in the basal plane. Due to the importance of carbon to oxygen (C/O) ratio and influence of oxygen-containing groups on the resulting rGO properties, the transformation of several functional groups has also gained research interest [103]. Numerous experiments on thermal reduction of GO have been performed under different annealing environments, ranging from inert to reducing and oxidizing gases, such as argon [104, 105], vacuum [106], hydrogen [107], ambient air [108-110], and nitrogen [111].

### **2.3.2 Properties of GO and rGO**

GO is characterized by facile dispersion in water and other organic solvents, as well as in different matrixes, which is attributed to the incidence of oxygen functionalities [112]. This property remains very crucial to the mixing of the material with ceramic or polymer matrixes in attempts to enhance their electrical, thermal and mechanical properties. Nonetheless, in terms of electrical conductivity, GO is typically

described as an electrical insulator due to the disruption of its  $sp^2$  bonding complex [112].

The GO is reduced to improve its honeycomb hexagonal lattice, and its derivative electrical conductivity. It should be considered that the removal of the bulk of oxygen groups, the resulting rGO is more difficult to disperse due to its tendency to aggregate [113]. Functionalization of GO can basically alter its properties to produce chemically modified graphene that can be potentially adapted for a wide range of applications. There are many ways in which GO can be functionalized, depending on the desired application. In the manufacture of optoelectronics and biodevices, or as a drug-delivery material, chemically modified graphene can be functionalized with amines to increase its dispersibility in organic solvents. Porphyrin-functionalized primary amines and fullerene-functionalized secondary amines have been conjugated with GO platelets to enhance nonlinear optical performance [113].

Elucidating the lattice and electronic band structures of graphene, GO and rGO is requisite to understand how the transformation of GO to rGO results in high photoexcitation response. The atomic structure of GO is apparently a graphene basal plane affixed with randomly distributed oxygen-bearing functional groups (hydroxy and epoxy units) leading to the formation of a  $sp^3$  matrix (Fig. 2.4 (a)) which makes GO an electronic insulator [114]. The electronic band structures of GO and rGO are depicted in Figure 2.4 (b) and (c), respectively. The initially structured hexagonal lattice of graphene becomes distorted by oxygenous defects generated during chemical oxidization.

The optoelectronic properties of carbon materials comprising a mixture of  $sp^2$  and  $sp^3$  bonds are principally controlled by  $\pi$  and  $\pi^*$  states of  $sp^2$  locations, lying in  $\sigma$ – $\sigma^*$  gap [115, 116]. Given that  $\pi$  bonding is relatively weaker with low formation energy, it is likely that many disorder-induced localized states may emerge within the 2D complex of as synthesized GO [116]. The structural disorder-induced localized states possibly exist in the band tail of  $\pi$ – $\pi^*$  gap or are present deep within this gap. Therefore, optical transitions relating to these disorder-induced localized states may initiate wide absorption or emission bands [115, 116]. Nonetheless, the reduction process causes the number of disorder-induced states to decrease due to deoxygenation. This structural transformation is due to the reduction of oxygenous functional groups and slow resurgence of the conjugate bonds between carbon atoms during the reduction process [116, 117]. Consequently, certain carbon lattices from the initial disrupted  $sp^2$  domains may expand the graphitic domains of  $sp^2$  clusters [116, 117]. These small  $sp^2$  clusters then generate isolated or discrete molecular states that percolate to enable the transport of charge carriers by hopping [114]. Hence, the reduction process results in a number of outcomes that include improved carrier mobility, higher absorption, a tunable band-gap where photoresponsivity can be adjusted by controlling the level of defects and presence of oxygen groups [114, 116, 118].

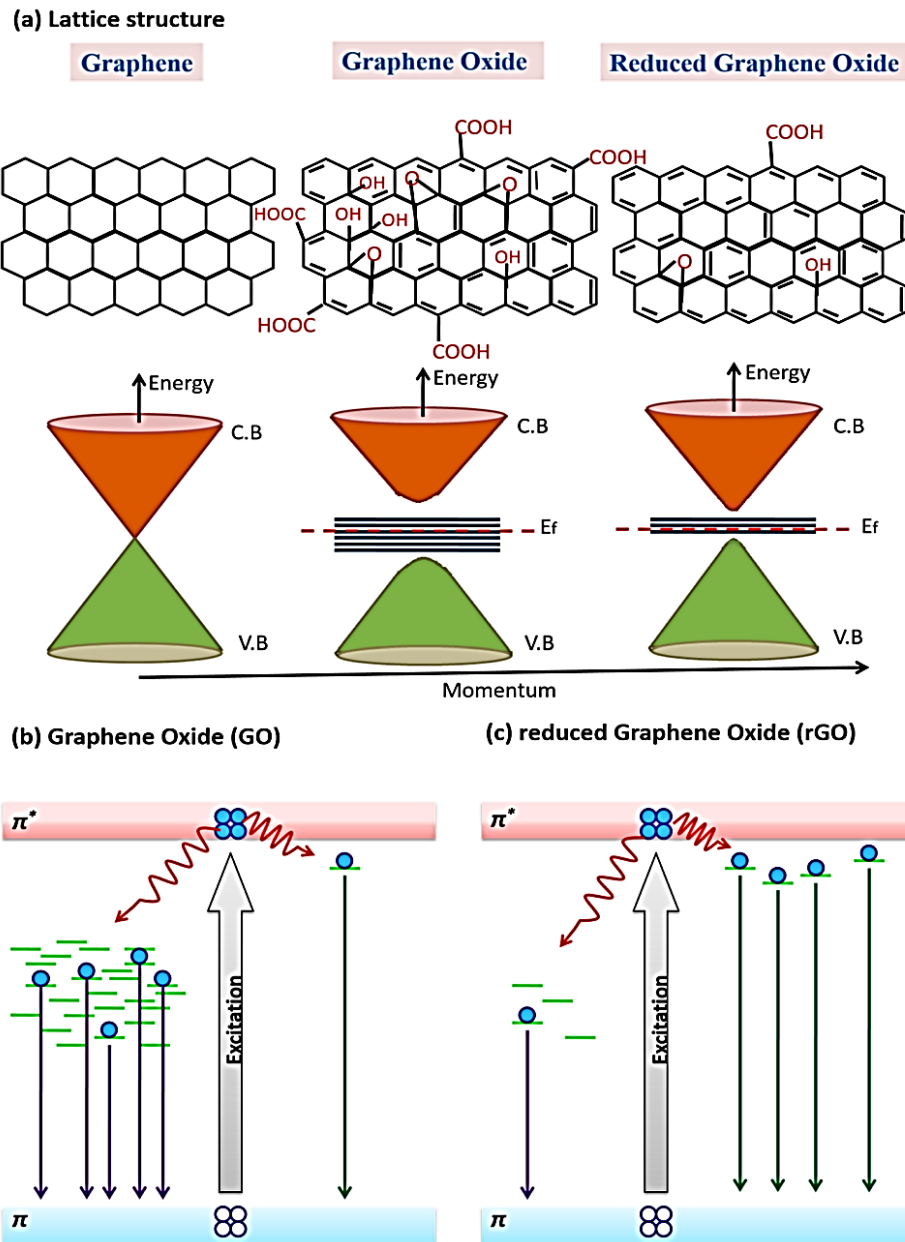


Figure 2.4 Schematic representation of: (a) Lattice structure and corresponding energy band diagrams of graphene, GO and rGO; and electronic transitions in (b) GO and (c) rGO[119].



### 2.3.2(a) Mechanical properties

The attractive mechanical properties of the pristine graphene monolayer graphene is well-reported it is recorded as having a break intensity of 42 Nm<sup>1</sup>, 1.0 TPa Young's modulus, and an inherent tensile force Up to 130.5 GPa [120]. Graphene's fracture toughness has also been researched by Zhang et al., and was confirmed to be as small as  $4.0 \pm 0.6 \text{ MPa m}^{1/2}$ , which confirms the low fracture of sheets of graphene [121]. In an attempt to attain these, GO and rGO blends were made. Suk et al. [122] reported monolayer GO (produced by means of a modified Hummer's method) with a Young's modulus of  $207.6 \pm 23.4 \text{ GPa}$ , a decrease in order-of-magnitude but still especially high. Similarly, Gomez-Navarro et al. reported an rGO monolayer, produced using the original Hummer's method followed by thermal annealing in a hydrogen environment, with a Young's modulus of  $250 \pm 150 \text{ TPa}$  [123]. Polymer nanocomposites benefit greatly from the use of GO and its derivatives as fillers [124].

### 2.3.2(b) Electrical properties

Graphene is electrically conductive with high electron mobility ( $25 \text{ m}^2 \text{ V}^{-1} \text{ s}^{-1}$ ) [125] and electrical conductivity ( $6500 \text{ S m}^{-1}$ ) [126]. Graphene has been employed to significantly enhance the electrical conductivity of polymers at low filler contents (e.g.,  $0.1 \text{ S m}^{-1}$  at 1 vol% in polystyrene (PS) [127]. However, the process of fabricating GO leads to the distortion of the  $\text{sp}^2$  bonding orbitals of graphene and the inclusion of surface functional groups that hinder its electrical conductivity, which increases the electrical resistivity of GO ( $1.64 \times 10^4 \text{ } \Omega \text{ m}$ ) [128, 129]. Due to this high resistivity, different techniques of GO reduction into rGO have been explored.

The reduction process significantly improves the electrical conductivity of GO, allowing it to be tuned over several orders of magnitude with conductivities ranging from  $\sim 0.1 \text{ S m}^{-1}$  [130] to  $2.98 \times 10^4 \text{ S m}^{-1}$  [91]. However, the rGO still contains residual  $\text{sp}^3$  bonded carbon to oxygen after reduction, which impedes the mobility of charge carriers through the other  $\text{sp}^2$  clusters. The transport electric charges in rGO occurs mainly by means of hopping, which is different from that of mechanically exfoliated graphene [131]. Given the need to optimally reduce GO, several attempts have been made to improve the synthesis of electrically conductive rGO. For instance, Stankovich et al [132] utilized hydrazine hydrate to reduce colloidal suspension of exfoliated GO in water. The resulting rGO displayed an electrical conductivity of  $2 \times 10^2 \text{ Sm}^{-1}$ , indicating the conductivity of GO was improved by 5 orders of magnitude after reduction.

### **2.3.2(c) Thermal properties**

Similar to its electrical conductivity, GO synthesized from graphite is characterized by a low thermal conductivity of  $0.5\text{--}1 \text{ Wm}^{-1}\text{K}^{-1}$ , which makes it a poor option for most applications that demand good thermal properties [133]. In contrast, graphene material is proven to have one of the highest in-plane thermal conductivities, across the range of  $\sim 3000\text{--}5000 \text{ Wm}^{-1}\text{K}^{-1}$  [127, 134]. Therefore, reduction of GO to rGO is vital for a number of applications. For example, rGO can be incorporated into polymers to enhance their thermal conductivity [135]. Renteria et al. [133] demonstrated that the synthesis of rGO films via annealing GO at high temperature ( $1000 \text{ }^\circ\text{C}$ ) can considerably enhance their in-plane thermal conductivity from  $\sim 3$  to  $61 \text{ Wm}^{-1}\text{K}^{-1}$ . The rGO films exhibited anisotropic thermal conductivity, as the cross-plane thermal conductivity reduced to  $\sim 0.09 \text{ Wm}^{-1}\text{K}^{-1}$  and showed an in-plane/cross-plane

thermal conductivity ratio of 675. This may prove valuable for specific applications that utilize directional heat conduction.

### **2.3.3 Application of GO and rGO**

The demand for flexible electrodes and strain sensors has grown tremendously because of the simplicity of their integration with non-conventional interfaces. In this regard, two main strategies have been implemented. One strategy involves the deposition or casting of layered thin films on a flexible substrate, while the other strategy uses flexible composite films. Both strategies have been explored at length, with each having its niche areas of applications. Layered films have been utilized for optoelectronic and device applications like solar cells [123], transistors [124], light emitting diodes (LEDs) [136], lasers [137], photodetector [126], biosensor [138], biomedical [139], water purification [140], and photocatalysis [141]. In these regards, the energy band alignment and the ease of interfacing are needed, due to the exceptional electrical and optical properties of graphene.

Among these numerous applications, considerable efforts have been focused on the study for optoelectronic applications. Specifically, the study of free-standing GO has recently emerged as a popular area of research, with focus being on enhancing both highly electrically conductive and highly porous GO structures because of their flexibility and high mechanical strength. And these make them viable materials for energy storage [142-144], conductor applications [145], and environmental applications [146, 147].

However, prior research has not considered the potential effects of optoelectronic properties and applications for GO. Studies on the nanoscale to microscale syntheses of these novel 2D materials have rarely considered them as viable